Forbidden Band Gaps in the Spin-Wave Spectrum of a Two-Dimensional Bicomponent Magnonic Crystal

S. Tacchi,[1,*] G. Duerr,[2] J. W. Klos,[3] M. Madami,[1] S. Neusser,[2] G. Gubbiotti,[1,4] G. Carlotti,[1,5] M. Krawczyk,[3] and D. Grundler[2,†]

[1]CNISM, Unità di Perugia and Dipartimento di Fisica, Via A. Pascoli, I-06123 Perugia, Italy
[2]Lehrstuhl für Physik funktionaler Schichtsysteme, Technische Universität München, Physik Department, James-Franck-Strasse 1, D-85747 Garching bei München, Germany
[3]Faculty of Physics, Adam Mickiewicz University, Umultowska 85, Poznań, 61-614, Poland
[4]Istituto Officina dei Materiali del CNR (CNR-IOM), Unità di Perugia, c/o Dipartimento di Fisica, Via A. Pascoli, I-06123 Perugia, Italy
[5]Centro S3, CNR-Instituto di Nanoscienze, Via Campi 213A, I-41125 Modena, Italy

(Received 21 June 2012; published 28 September 2012)

The spin-wave band structure of a two-dimensional bicomponent magnonic crystal, consisting of Co nanodisks partially embedded in a Permalloy thin film, is experimentally investigated along a high-symmetry direction by Brillouin light scattering. The eigenfrequencies and scattering cross sections are interpreted using plane wave method calculations and micromagnetic simulations. At the boundary of both the first and the second Brillouin zones, we measure a forbidden frequency gap whose width depends on the magnetic contrast between the constituent materials. The modes above and below the gap exhibit resonant spin-precession amplitudes in the complementary regions of periodically varying magnetic parameters. Our findings are key to advance both the physics and the technology of band gap engineering in magnonics.

DOI: 10.1103/PhysRevLett.109.137202 PACS numbers: 75.30.Ds, 75.40.Gb, 75.78.−n, 78.35.+c

Magnonic crystals (MCs) are a new class of metamaterials where a periodic modulation of magnetic properties allows for manipulation of the band structure of spin waves (SWs) [1–3]. This is similar to photonic crystals [4], where allowed frequency bands and forbidden frequency gaps (band gaps) are tailored for light by a smart choice of the geometrical symmetry and/or the materials [5]. For two-dimensional (2D) photonic crystals, air holes periodically arranged in a dielectric film have been a powerful concept to induce the Bragg reflection of light. Contrarily to electromagnetic waves, SWs, i.e., the low lying excitations in magnetically ordered substances, do not exist in air, and the incorporation of a second magnetic material is key to provide the relevant material contrast for continuously propagating SWs in MCs. Such so-called bicomponent magnonic crystals (BMCs) offer magnonic band structures that can be tuned by changing either the spatial symmetry, the filling fraction, or the magnetic contrast of constituent materials [6–10]. Pioneering experiments have been focused on 1D BMCs consisting of an array of longitudinally magnetized Co and $Ni_{80}Fe_{20}$ (Py) alternated nanostripes [11,12]. Here, the Co stripes exhibited forced spin precession, thereby enhancing the dynamic dipolar coupling between confined modes in the Py stripes [11–13]. Very recently, it has been shown that propagation of SWs in 2D bicomponent antidot lattices is guided into channels of nanometric width which reside in complementary regions depending on the eigenfrequency [14]. In the case of a 2D chessboardlike square array of dots [15], the periodically modulated internal fields and damping parameters were decisive to understand the modes. A band gap for SWs at Brillouin zone (BZ) boundaries, however, was not observed, and it is an open question whether SWs in such 2D BMCs reflect the magnetic-contrast-induced band formation due to different material parameters. In this Letter, the SW dispersion along one of the principal symmetry directions in a 2D BMC, consisting of Co nanodisks (so-called dots) partially embedded in a Py thin film, has been measured by Brillouin light scattering (BLS). The experimental data are successfully explained by both micromagnetic simulations and plane wave method (PWM) calculations. We find that the composite structure supports propagating modes whose spatial profiles are calculated and discussed. Evidence is given for the opening of band gaps, caused by Bragg diffraction of SWs induced by the magnetic contrast effect, creating great perspectives for tailored band structures in magnonics similar to photonics and electronics.

The bicomponent investigated sample consists of a square lattice of shallow circular holes (8 nm deep) etched into a 24 nm thick Py film and filled with 15 nm thick Co dots [Fig. 1(a)]. The Co dot radius is $R = 155$ nm, and the lattice parameter is $a = 600$ nm. The corresponding first BZ is a square of side length $2q_{BZ} = 2\pi/a = 1.046 \times 10^5$ rad/cm. The dispersion of SW modes has been measured by BLS for the in-plane transferred wave vector (q_y) up to 1.8×10^5 rad/cm, i.e., up to the fourth BZ. The magnetic field $H_0 = 200$ Oe was applied along the z axis perpendicularly to q_y.

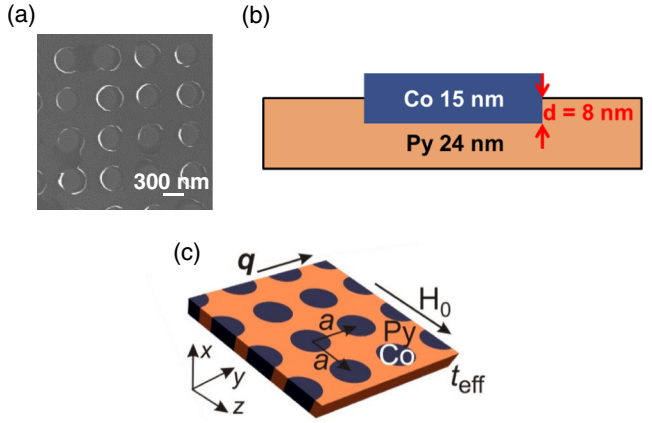

FIG. 1 (color online). (a) Scanning electron micrograph of the binary component dot-antidot lattice. (b) Schematic cross section of the sample showing a 15 nm thick Co nanodisk embedded in a 24 nm thick Py film. This is used for micromagnetic simulations. (c) Picture of the BMC structure used in PWM calculations. The sample is uniform across the thickness t_{eff}. The lattice constant is a.

Open circles in Fig. 2(a) represent the measured SW frequencies as a function of the transferred wave vector. In the first BZ, we detect several discrete peaks showing a clear dispersive character. These modes merge into one branch in the second BZ. Magnonic forbidden frequency gaps, having widths of 0.6 and 0.3 GHz, are observed at the boundaries of the first and second BZs, respectively.

The SW dispersion has been calculated by means of the MICROMAGUS micromagnetic package, using 2D periodic boundary conditions [16]. To reproduce the sample composition, we simulated a structure composed by three different layers: a 16 nm thick bottom layer consisting only of Py, an 8 nm thick middle layer consisting of Co dots fully embedded in Py, and a 7 nm thick top layer consisting only of Co dots. The lattice constant and the radius of Co dots have been set to their nominal values. The

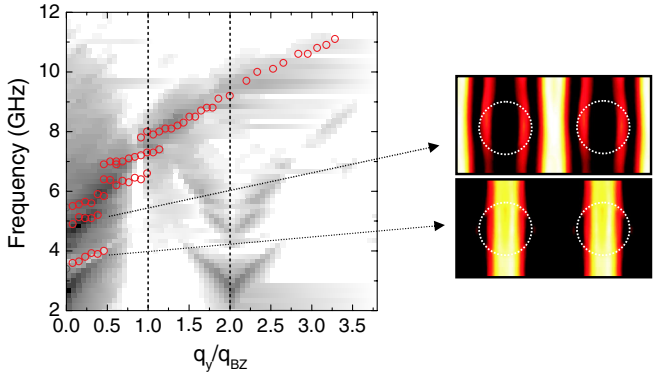

FIG. 2 (color online). Measured (open circles) and simulated (gray scale plot) mode frequencies as a function of the SW wave vector. Right side: spatial spin-precession profiles of two modes calculated at $q_y/q_{\text{BZ}} = 0.19 \times 10^{-5}$. Bright color indicates large spin-precession amplitude.

simulated structure had a size of 19.2 μm by 600 nm in the y and z directions, respectively. The sample is excited by a 0.05 ns long field pulse with 2 Oe amplitude projected onto both the x and z directions. The time resolved evolution of the magnetization is recorded over a period of 6 ns. To obtain the dispersion relation, a temporal and spatial fast Fourier transform of the x component of the magnetization, averaged in the z direction, is performed [17].

The saturation magnetizations and the exchange constants have been fixed to the values of $M_{\text{S,Py}} = 0.78 \times 10^6$ A/m, $A_{\text{Py}} = 1.3 \times 10^{-11}$ J/m and $M_{\text{S,Co}} = 1.0 \times 10^6$ A/m, $A_{\text{Co}} = 2.0 \times 10^{-11}$ J/m for Py and Co, respectively [18]. In Fig. 2, the micromagnetic simulations (gray scale plot) are shown together with the BLS frequencies. In the simulations, we find two pronounced dispersive branches (dark areas), whose frequencies agree quite well with experimental data. Corresponding spatial spin-precession profiles for $q_y/q_{\text{BZ}} = 0.19 \times 10^{-5}$, i.e., close to the Γ point, are shown on the right side of Fig. 2. The lower frequency mode extends in the vertical stripes going through both Py and Co, while the higher frequency one resides in the Py vertical stripes. Note that the SWs are uniform throughout the sample thickness and that the dispersions extracted from the three layers considered in the simulations exhibit identical behavior (data not shown); only the relative intensities of the two prominent modes were found to be different. Because of the restricted resolution of micromagnetic simulations, the forbidden frequency gap at the boundary of the first BZ is not clearly resolved.

To better understand the SW band structure, the PWM [19], especially appropriate for solving harmonic-in-time excitation in periodic structures, is applied. The SW dispersion relation is determined from the Landau-Lifshitz (LL) equation: $\frac{\partial \mathbf{M}}{\partial t} = -\gamma\mu_0[\mathbf{M} \times \mathbf{H}_{\text{eff}}]$, where $\mathbf{M}(\mathbf{r}, t)$ is the magnetization vector, γ is the gyromagnetic ratio, μ_0 is the permeability of vacuum, $\mathbf{r}$ is a position vector in the plane of a BMC, and t is time. $\mathbf{H}_{\text{eff}}$ is the effective magnetic field, which can be written as $\mathbf{H}_{\text{eff}}(\mathbf{r}, t) = \mathbf{H}_0 + \mathbf{H}_{\text{ex}}(\mathbf{r}, t) + \mathbf{H}_{\text{ms}}(\mathbf{r}, t)$, where $\mathbf{H}_0$ is the applied static magnetic field; $\mathbf{H}_{\text{ex}} = \nabla l_{\text{ex}}^2 \nabla \mathbf{m}(\mathbf{r}, t)$ is the exchange field, with $l_{\text{ex}} = \sqrt{2A/\mu_0 M_S^2}$; and $\mathbf{H}_{\text{ms}}$ is the magnetostatic field, which has been calculated following the procedure described in Refs. [20,21]. To solve the linearized LL equation, we assume the dynamical magnetization to take the Bloch wave form $\mathbf{m}(\mathbf{r}, t) = \sum_{\mathbf{G}} \mathbf{m}_{\mathbf{q}}(\mathbf{G}) e^{i(\mathbf{q}+\mathbf{G})\cdot\mathbf{r}} e^{i\omega t}$, where $\mathbf{G}$ is a reciprocal lattice vector, $\mathbf{q}$ is the wave vector, and ω is the angular frequency of a SW.

By writing the LL equation in the reciprocal space, an eigenvalue problem for frequencies ω and $\mathbf{m}_q(\mathbf{G})$, being eigenvalues and eigenvectors, respectively, is obtained. For a spin-wave mode, the inelastic light scattering intensity I is determined by the component of the dynamical magnetization perpendicular to the BMC structure, so the BLS intensity is given by the squared amplitude of the Fourier component

$m_{x,q}(\mathbf{G} = \mathbf{0})$ for the specific mode $I \propto |\boldsymbol{m}_{x,\mathbf{q}}(0)|^2$ [22]. In the PWM calculations, we modeled our system as a BMC having a uniform structure and an effective thickness t_{eff}, whereas the composition of our sample is not uniform [Fig. 1(b)]. We find $t_{\text{eff}} = 20$ nm to provide the best agreement with the experimental results, while the lattice constant and the radius of Co dots have been set to their nominal values [Fig. 1(c)]. To test the validity of such an approximation, we evaluated the static demagnetizing field in our system. We found that the profile of the demagnetizing field is preserved across the thickness; therefore, the utilization of a uniform BMC in PWM is justified to a large extent. Because of the small overall thickness of our Co/Py BMC (much smaller than the lattice constant), SW modes considered in this work are characterized by a uniform profile across the thickness, in agreement with the results of the micromagnetic simulations discussed above. The saturation magnetization and the exchange constant of Co and Py have been fixed to the values used in the micromagnetic simulations. In all calculations, the bias field $H_0 = 200$ Oe was directed along the z axis [Fig. 1(c)].

The magnonic spectra calculated by the PWM, superimposed with the BLS data (black dotted lines and open circles, respectively), are shown in Fig. 3(a). The PWM-calculated spectra are richer and denser than the experimental ones (the bold lines mark the calculated bands with the largest intensities). As can be seen, a good agreement is found between the BLS data and the most intense lines calculated by the PWM (which also agree with the prominent branches found in the micromagnetic simulations). However, the BLS data do not exactly follow the branch marked as the most prominent one in the PWM results, but still reflect dispersive modes within the first BZ with the group velocity, $v_g > 0$. Such a discrepancy might be due to the fact that, in PWM calculations, only the components of the static stray field collinear with $\mathbf{H}_0$ are considered. Further components of the stray field and slightly noncollinear arrangements of magnetic moments are neglected (cf. Fig. 4 in Ref. [14]).

In Fig. 3(b), we show the calculated magnonic band structure limited to the low frequency modes in the first BZ, which can be classified by taking into account their spatial profiles. (i) Modes analogous to the surface Damon-Eshbach (DE) mode of a continuous film [labeled 1, 2, and 3 in Fig. 3(b)]. At the Γ point, the spatial profile of the component m_x is not uniform, but it is influenced by the modulation of the internal field, having the same periodicity as the artificial lattice constant. Therefore, these modes extend in effective stripes going through either Co dots and Py (modes 1 and 2) or the Py alone, thereby bypassing the Co dots (mode 3). Modes 1 and 2 are found to exhibit a frequency lower than mode 3 because the static demagnetizing field in the Co dots is opposite to $\mathbf{H}_0$ [14]. It is important to note that, at the Γ point, the v_g of mode 1 (4.3 km/s) is larger than that of mode 3 (2.4 km/s)

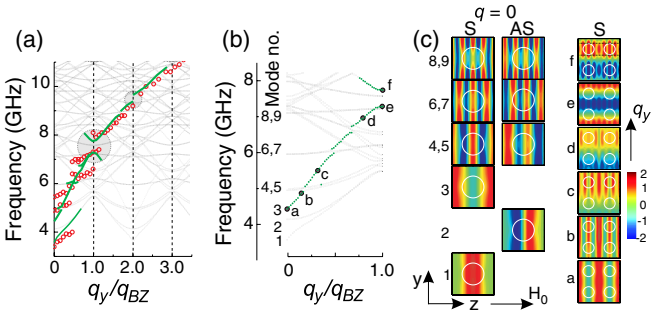

FIG. 3 (color online). (a) Magnonic band structure of the Co/Py 2D BMC calculated by the PWM (black dotted lines). The bold solid lines mark the calculated bands with the largest intensities. We replot the BLS data from Fig. 2 as open circles. Filled gray circles highlight the magnonic gaps opened at the 1st and 2nd BZ boundaries (indicated by vertical dashed lines). (b) The enlarged part of the calculated magnonic band structure from the 1st BZ shown in (a). The modes are numbered from 1 to 9 according to arrangements at the center of the BZ. (c) Left panel: x components of the magnetization vector, m_x, for modes 1 to 9. Right panel: evolution of mode 3 for wave vector values $q_y/q_{BZ} = 0$, 0.18, 0.34, 0.8, and 1, as indicated by filled dots and indexed with small letters from a to f in (b). In points e and f, the horizontal broken lines indicate the regions where the stationary waves have the maximum of the spin precessional motion.

because the former propagates in the effective stripes where the internal magnetic field is lower and the saturation magnetization is higher due to the presence of the Co dots if compared to the Py stripes where mode 3 is localized [23]. Remarkably, the modes show either a symmetric (S, modes 1 and 3) or antisymmetric (AS, mode 2) character with respect to the xy plane through the center of the Co dots. Moving from the Γ point toward the first BZ boundary, modes 3 and 1 have a similar cross section, while, in the second and third BZs, mode 3 becomes the most intense excitation and the only mode detected in the BLS measurements. This is due to the fact that they assume a marked DE character, i.e., an oscillating behavior along the y direction [see the profiles in points b, c, d, e, and f of Fig. 3(c)]. (ii) Backwardlike (BA) modes, characterized by several nodal planes perpendicular to the direction parallel to $\mathbf{H}_0$, reflecting standing SWs which are higher-order modes of the magnetostatic backward volume wave type [24]. Strikingly, their frequencies are higher than those of modes 1 to 3 at the Γ point and increase with the number of nodal planes. This is expected for magnetostatic backward volume waves if one resides in the exchange-dominated regime of the SW dispersion relation. Such modes always exist in pairs which have the same periodicity and are almost degenerate in frequency [modes 4 and 5, 6 and 7, and 8 and 9 in Fig. 3(c)]. The magnetization precession of the lower (higher) frequency mode of every pair is S (AS) with respect to the xy plane through the center of the Co dots. (iii) Modes at frequencies larger than 7 GHz, which are not numbered in Fig. 3(b). These modes are characterized by

several oscillations of the dynamical magnetization in both parallel and perpendicular directions to the applied field. Their classification is difficult and ambiguous due to the large density of modes and their consequent hybridization.

As can be seen in Fig. 3(c), the spatial profile of mode 3 is strongly affected by interaction with the BA modes. In particular, it hybridizes (anticrosses) with the S modes (modes 4, 6, and 8), changing its spatial profile, whereas it does not interact (it crosses) with the AS ones (modes 5, 7, and 9). Note that, after the hybridization with mode 4, mode 3 becomes a mode which is no longer restricted to Py stripes but spreads through the whole matrix. The anticrossings provoke tiny frequency gaps in branches within the first BZ that are different from the gaps at BZ boundaries in that the group velocity does not become zero at the relevant wave vectors. The PWM highlights that anticrossings and hybridization effects are prominent features in the 2D BMC band structure. Importantly, the PWM reproduces very well the widths of the band gaps of about 0.6 and 0.3 GHz observed for DE-like modes at the boundaries of the first and second BZs in BLS, respectively [gray areas in Fig. 3(a)] [25]. Following the PWM results, the periodic modulation of the magnetic material properties gives rise to Bragg diffraction, i.e., counterpropagating ''Bragg-reflected'' waves. Mode 3 experiences, in particular, the periodicity of the magnetic structure, and, as a consequence, two stationary waves with wavelengths $2a$ are formed, which differ by a spatial shift corresponding to half of the lattice constant. At the boundary of the first BZ, the higher frequency mode [point f in Figs. 3(b) and 3(c)] has a maximum of the spin precessional motion in the horizontal stripes containing Co dots, while the lower frequency mode [point e in Figs. 3(b) and 3(c)] has the maximum in horizontal Py stripes comprised between the Co dots.

Finally, to achieve a deeper insight into the roles of both the magnetic contrast between Co and Py and the geometrical parameters of the structure, an analytical equation for the SW frequencies at the BZ boundaries is derived, assuming $G_z = 0$ and $q_z = 0$, i.e., neglecting the nonuniformity along the z axis. Starting from the PWM equations used for solving the LL equations, we follow ideas known from approximate calculations of photonic and electronic band gap widths by Kittel [26] and Yariv *et al.* [27]. Under such conditions, $\mathbf{m}_{qy}(G = 0)$ and $\mathbf{m}_{qy}(G = G_n)$ are the dominant terms in the Fourier expansions of the dynamical magnetization components at the boundaries of the nth BZ ($n = 1, 2, \ldots$) along q_y, and therefore the SW frequencies can be expressed as

$$\omega_{\mp} = \gamma\mu_0\left(\sqrt{\{H_0 + C(q_y)[M_S(0) \mp M_S(G_n)]\}}\sqrt{\{H_0 + [1 - C(q_y)][M_S(0) \mp M_S(G_n)]\}}\right), \quad (1)$$

where $C(q_y) = \frac{1-e^{-|q_y|t_{\mathrm{eff}}}}{2}$. The Fourier coefficients of the saturation magnetization in the 2D BMC are $M_S(0) = (M_{S,Co} - M_{S,Py})f + M_{S,Py}$ and $M_S(G_n) = 2(M_{S,Co} - M_{S,Py})f\frac{J_1(G_nR)}{G_nR}$, where J_1 is a Bessel function of the first kind and $f = \pi R^2/a^2$ is the filling fraction of Co in Py. Such an approximation can be justified because, at the boundary of both the first and second BZs, the spatial profile of mode 3 is almost uniform along the z axis. Using Eq. (1), we obtain a value of the gap width at the boundary of the first (second) BZ of 0.5 (0.14) GHz, in quite good agreement with the full PWM calculation (0.45 and 0.15 GHz). From Eq. (1), we find that the width of the band gap increases almost linearly with the magnetic contrast, i.e., $M_{S,Co} - M_{S,Py}$. For a given lattice, it is influenced by the thickness and filling fraction f. Equation (1) predicts the maximum band gap width of 0.67 GHz to occur at $f = 0.46$ ($R = 230$ nm). Note that the amplitude of the demagnetizing field is almost constant along vertical lines (i.e., along the y axis where the peak-to-peak variation is only about 20 Oe) and does not contribute significantly to the opening of the forbidden frequency gap [28]. This is different than recent reports on band gap creation in both conventional antidot lattices [29] and width-modulated magnonic waveguides subject to in-plane magnetic fields [30], where a main role is played by large internal field variations provoked by air holes.

In conclusion, spin-wave propagation in a 2D BMC, consisting of Co dots partially embedded in a Py film, has been studied by BLS. A band gap of about 0.6 (0.3) GHz has been observed at the boundary of the first (second) BZ (induced by the Bragg diffraction of DE-like spin-wave modes), whose width has been quantitatively explained by the PWM in terms of the magnetic contrast between the Co and the Py.

S. T. and G. D. contributed equally to this work. The research leading to these results has received funding from the European Community (FP7/2007-2013) under Grant Agreement No. 228673 (MAGNONICS) and the German Excellence Cluster ''Nanosysteme Initiative Munich.''

*silvia.tacchi@fisica.unipg.it
†grundler@ph.tum.de

[1] S. A. Nikitov, Ph. Tailhades, and C. S. Tsai, J. Magn. Magn. Mater. **236**, 320 (2001).
[2] V. V. Kruglyak *et al.*, in *Metamaterial*, edited by Xun-Ya Jiang (InTech, Open Access, 2012), ISBN .
[3] G. Gubbiotti, S. Tacchi, M. Madami, G. Carlotti, A. O. Adeyeye, and M. Kostylev, J. Phys. D **43**, 264003 (2010).

[4] J. Joannopoulos, P. Villeneuve, and S. Fan, Solid State Commun. **102**, 165 (1997).
[5] B. Lenk, H. Ulrichs, F. Garbs, and M. Munzenberg, Phys. Rep. **507**, 107 (2011).
[6] J. O. Vasseur, L. Dobrzynski, B. Djafari-Rouhani, and H. Puszkarski, Phys. Rev. B **54**, 1043 (1996).
[7] M. Krawczyk and H. Puszkarski, Phys. Rev. B **77**, 054437 (2008).
[8] F. S. Ma, H. S. Lim, Z. K. Wang, S. N. Piramanayagam, S. C. Ng, and M. H. Kuok, Appl. Phys. Lett. **98**, 153107 (2011).
[9] C. S. Lin, H. S. Lim, Z. K. Wang, S. C. Ng, and M. H. Kuok, Appl. Phys. Lett. **98**, 022504 (2011).
[10] F. S. Ma, H. S. Lim, V. L. Zhang, Z. K. Wang, S. N. Piramanayagam, S. C. Ng, and M. H. Kuok, J. Appl. Phys. **111**, 064326 (2012).
[11] Z. K. Wang, V. L. Zhang, H. S. Lim, S. C. Ng, M. H. Kuok, S. Jain, and A. O. Adeyeye, ACS Nano **4**, 643 (2010).
[12] V. L. Zhang, H. S. Lim, C. S. Lin, Z. K. Wang, S. C. Ng, M. H. Kuok, S. Jain, A. O. Adeyeye, and M. G. Cottam, Appl. Phys. Lett. **99**, 143118 (2011).
[13] C. S. Lin, H. S. Lim, V. L. Zhang, Z. K. Wang, S. C. Ng, M. H. Kuok, M. G. Cottam, S. Jain, and A. O. Adeyeye, J. Appl. Phys. **111**, 033920 (2012).
[14] G. Duerr, M. Madami, S. Neusser, S. Tacchi, G. Gubbiotti, G. Carlotti, and D. Grundler, Appl. Phys. Lett. **99**, 202502 (2011).
[15] G. Gubbiotti, S. Tacchi, M. Madami, G. Carlotti, S. Jain, A. O. Adeyeye, and M. P. Kostylev, Appl. Phys. Lett. **100**, 162407 (2012).
[16] D. V. Berkov and N. L. Gorn, computer code MICROMAGUS, 2008.
[17] V. V. Kruglyak and R. Hicken, J. Magn. Magn. Mater. **306**, 191 (2006).
[18] These parameter values are different from Ref. [14]. In Ref. [14], only data at $q = 0$ were at hand. Now, the parameters are chosen such that they remodel both the field and wave vector dependencies of eigenfrequencies.
[19] J. P. Boyd, *Chebyshev and Fourier Spectral Methods* (Dover, New York, 2000), 2nd ed.
[20] J. W. Klos, M. Krawczyk, and M. L. Sokolovskyy, J. Appl. Phys. **109**, 07D311 (2011).
[21] J. Kaczer and L. Murtinova, Phys. Status Solidi A **23**, 79 (1974).
[22] C. Mathieu *et al.*, Phys. Rev. Lett. **81**, 3968 (1998).
[23] D. D. Stancil and A. Prabhakar, *Spin Waves Theory and Applications* (Springer, New York, 2009).
[24] Note that the dispersion (slope) of BA-like modes is typically smaller than for DE-like modes in the long wavelength limit, so the frequency separations between successive standing SWs of the BA type are relatively small.
[25] Note that the SW mode which is inside the magnonic gap at the boundary of the first BZ has a negligible calculated cross section and is not active in the scattering process. Still, the band gap is a partial one, as further bands exist at the same energy at smaller and larger wave vectors. In photonics, it has been shown that lattice symmetries and filling fractions need to be optimized to obtain full band gaps [4].
[26] C. Kittel, *Introduction to the Solid State Physics* (Wiley, New York, 1996).
[27] A. Yariv and P. Yeh, *Optical Waves in Crystals* (Wiley-Interscience, New York, 2003), p. 156.
[28] We have investigated a further 2D BMC with $R = 215$ nm for the Co dots and $a = 1000$ nm. The BLS data (not shown) suggest a gap width at the boundary of the 1st BZ of only 0.27 GHz or even smaller. Equation (1) provides 0.36 GHz for this sample using the same material parameters.
[29] R. Zivieri *et al.*, Phys. Rev. B **85**, 012403 (2012).
[30] A. V. Chumak *et al.*, Appl. Phys. Lett. **95**, 262508 (2009).